Modelling and Aerodynamic Performance of an Unmanned Aerial Vehicle Wing

A. Isah[1,2*], M. S. Lawal[1], I. Yahuza[1], A. Na'inna[1]

[1]Automotive Engineering Department, Air Force Institute of Technology, Kaduna, Nigeria.
[2]Sustainable AeroDesign and Propulsion Research Group, Air Force Institute of Technology, Kaduna, Nigeria.

ABSTRACT: Over the decades, the number of unmanned aerial vehicles (UAVs) has increased due to their versatile applications. The aerofoil-formed wing is the primary lift-generating component of a fixed-wing aircraft. Incorporating a hybrid wing design and combining two different aerofoils can enhance aerodynamic performance. The Ichoku-18 (IU-18) UAV features such a configuration, using the NACA2415 aerofoil at the root and the SD7032 at the tip, along with geometric twist. This study developed computational fluid dynamics (CFD) models of an IU-18 UAV's wing and analyse its aerodynamic performance. The lift and drag coefficients, pressure distributions, and aerodynamic efficiency using realisable k-ε and SST k-ω turbulence models at angles of attack (AoA) of 0°-24° in four increments were investigated. At 0° AoA, the minimum drags coefficients predicted by the SST k-ω and realisable k-ε models were 0.015 and 0.016, respectively, within expected ranges. Furthermore, all models identified 16° as the critical AoA. As AoA increased, pressure on the wing increased while air velocity decreased, consistent with Bernoulli's principle, influencing lift and drag generation. Overall, this study enhances the understanding of the IU-18 UAV wing's aerodynamic behaviour and evaluates the accuracy of selected turbulence models under cruise conditions.

KEYWORDS: Unmanned Aerial Vehicle, Aerodynamics, Computational Fluid Dynamics, Drag coefficient, Lift coefficient.

[Received May 16, 2025; Revised June 29, 2025; Accepted July 3, 2025] Print ISSN: 0189-9546 | Online ISSN: 2437-2110

I. INTRODUCTION

The rapid expansion of unmanned aerial vehicles (UAVs) across civilian, industrial, and military sectors has spurred extensive research and development in this area. UAVs operated remotely or autonomously are designed to perform tasks in hazardous or challenging environments, reducing human risk (Bardera *et al.,* 2024; İnan and Ceylan, 2024; Zharif *et al.,* 2024). For decades, research has focused on optimising UAV performance, particularly wing geometry and aerofoil selection, which are critical to aerodynamic efficiency. Wings often incorporate varying aerofoil profiles from root to tip to enhance performance (Anderson, 2011; Cakir, 2012). Studies have shown that the angle of attack (AoA) has a more pronounced effect on wing performance than airspeed (Nigam *et al.,* 2017). Although modifications such as taper, twist, and sweepback contribute to performance, the aerofoil remains the primary source of lift. As AoA increases, surface pressure changes significantly, with effect on both lift and drag forces (Ismail *et al.,* 2020; Merryisha and Rajendran, 2019; Narendiranath *et al.,* 2017). According to Bernoulli's principle, lift results from the pressure difference between the upper and lower wing surfaces, while drag opposes motion. Therefore, accurate prediction of pressure distribution and aerodynamic forces is essential for wing performance evaluation (Iqbal *et al.,* 2025; Isah *et al.,* 2025; Lei *et al.,* 2024).

Computational fluid dynamics (CFD) has become a widely adopted tool in aerodynamic analysis due to its efficiency, cost-effectiveness, and ability to simulate complex flow phenomena. While wind tunnel testing remains valuable, it is often limited by scale and cost, making CFD a practical complementary research tool in aircraft design (Hasan *et al.,* 2025; Lawal *et al.,* 2015; Lei *et al.,* 2024). However, a major challenge in CFD analysis is getting high performance computers and selecting appropriate turbulence model for complex design (Mishra and Aharwal, 2018). Although models such as direct numerical simulation (DNS) and large eddy simulation (LES) are more accurate, their application to solve complex flows at high Reynolds number is not common due to demand for higher computing powers. Hence, the use of turbulence models-based Reynolds average Nervier Stokes Equations (RANS) is more common. Among the commonly used RANS models are Spalart-Allmaras, k-ε, and k-ω, each suited for specific applications. The Spalart-Allmaras model uses a single equation, while the k-ε and k-ω models are two-equation models (İnan and Ceylan, 2024; Isah *et al.,* 2022). The shear stress transport (SST) k-ω model is frequently recommended for its accuracy in predicting aerodynamic flow behaviour (Ali *et al.,* 2024).

Several studies have used CFD to analyze aerofoil and wing configurations. For instance, Kulshreshtha et al. (2020)

*Corresponding author: *dankade44@gmail.com*

doi: http://doi.org/10.63746/njtd.v22i4.3663

examined wings with NACA2412, 2414, and 2415 aerofoils at varying AoA employing steady-state approximation using the standard k-ε model. Siddiqi and Lee (2019) evaluated subsonic UAV wings using the Spalart-Allmaras, realizable k-ε, and SST k-ω models, identifying the Eppler 559 aerofoil as suitable for non-rectangular planforms. Bardera et al. (2024) studied rectangular UAV wings with Eppler 186 aerofoils modified with tubercles using the SST k-ω model. Their results, from AoA -5° to +30° in 5° increments, showed improved lift and delayed stall. A configuration with 0.05c amplitude and 0.25c wave length achieved a 17% increase in maximum lift coefficient and delayed stall to 20 ° AoA compared to the baseline. Ali et al. (2024) examined a leading-edge tubercle wing for low Reynolds number (Re) flows across AoA from 0° to 20° using five turbulence models. Results from the Stress-W RSM model predicted coefficients closest to experimental values, followed by realizable k-ε, SST, SST k-ω, and transition k-kl-ω models. At higher AoA (16° and 20°), the SST k-ω model yielded the most accurate predictions.

Yuichi et al. (2020) studied a multi-slotted high-lift wing for short take-off and landing (STOL) applications, demonstrating improved lift and delayed stall, but noting adverse effects from wing-tip vortex interactions. Eftekhari et al. (2019) assessed a NACA0012 wing at low Re using the Spalart-Allmaras model. Their results showed an increasing drag with AoA up to stall at 32°, followed by lift loss, with a 3% error below 15°AoA and 19% at 20° due to leading-edge flow separation. Arunkumar et al. (2018) used the SST $k-\omega$ model to evaluate winglet designs, finding that blended winglets improved lift and reduced drag, increasing fuel efficiency by 6-8%. Roy et al. (2018) also applied the SST $k-\omega$ model to a NACA4415 wing and found it accurately predicted boundary layer behavior, with increased AoA advancing stall and separation points toward the leading edge. These studies underscored the effectiveness of CFD and the significant impact of wing aerodynamic performance.

The Ichoku-18 (IU-18) UAV was analytically designed to meet specific performance requirements but lacks validation through CFD or wind tunnel testing. This study partly addresses this gap using CFD to predict the wing's aerodynamic performance. The novel wing features a NACA2415 at the root and SD7032 at the tip with a geometric twist, balancing structural integrity and aerodynamic efficiency. The analysis is performed from 0° to 24° at an interval 4°increments. Changes in AoA were achieved by rotating the wing model to the incident free stream. This study developed CFD models of an IU-18 UAV's wing to analyse its aerodynamic performance. The results of the models are compared with analytical design data. This paper is organized as follows: Section I provides the background of the study and brief literature review, Section II outlines the methodology, Section III presents and discusses the results, and Section IV concludes with key findings and recommendations.

II. METHODOLOGY

This study employs the CFD to solve the RANS equations governing fluid flow. By numerically solving these equations under defined boundary conditions, flow characteristics over a specified geometry can be predicted (Khuntia *et al.,* 2018; Narendiranath *et al.,* 2017). The flow is presumed to be steady, turbulent, viscous, and incompressible. Accordingly, the RANS equations are used, where stream variables are separated into mean and fluctuating components (Aftab *et al.,* 2016). The total velocity of fluid flow, u_i, summation of its mean velocity $\overline{u_\iota}$ and fluctuating $\acute{u}_\iota$ components can be expressed as follows:

$$u_i = \overline{u_\iota} + \acute{u}_\iota \quad (1)$$

This decomposition also applies to other variables such as pressure and momentum, as shown in Equations 2 to 4:

$$p = \bar{p} + \acute{p} \quad (2)$$

The average form of the continuity and momentum equations are presented in Equation 3 and 4, respectively.

$$\frac{\partial}{\partial x_i}(\overline{u}_i) = 0 \quad (3)$$

$$\frac{D\overline{u}_i}{Dt} = -\frac{1}{\rho}\frac{\partial P}{\partial x_i} + \frac{\partial}{\partial x_j}\left[\mu\left(\frac{\partial \overline{u}_i}{\partial x_j} + \frac{\partial \overline{u}_i}{\partial x_i} - \frac{2}{3}\delta_{ij}\frac{\partial \overline{u}_k}{\partial x_k}\right)\right] + \frac{\partial}{\partial x_j}\left(-\overline{\acute{u}_\iota \acute{u}_j}\right) \quad (4)$$

where ρ, u and μ represent the fluid density, velocity, and dynamic viscosity. The expression $-\overline{\acute{u}_\iota \acute{u}_j}$ is the Reynolds stress tensor (RST), which accounts for turbulence effects and must be modelled since it cannot be directly computed in common turbulence models. The preference for a turbulence model depends on the flow characteristics (Roy *et al.,* 2018). The Reynolds number (Re), a dimensionless factor that denotes the fraction of inertial to viscous forces, guiding turbulence model selection, was computed using Equation 5.

$$Re = \frac{\rho V D}{\mu} \quad (5)$$

where V is free-stream velocity, and D is the characteristic length, typically the chord length for aerofoils or the Mean Aerodynamic Chord (MAC) for non-uniform wings (Ananda *et al.,* 2015). Fully turbulent flow is assumed for $R_e \geq 10^6$ (John and Russell, 2014).

Accordingly, understanding the abilities and limitations of the study and maintaining possible minimum computational time and resources, it is necessary to make the most appropriate choice of a turbulence model. At the cruising altitude, 4,572 m, the flow is predominantly turbulent, though low Re regions may appear, specifically at high AoA, where flow separation is expected.

For this study, the realizable k-ε and SST k-ω turbulence models were selected due to their effectiveness in such conditions to adequately analyse the flow around the IU-18 UAV wing. Previous studies have shown that the realizable k-ε model performs well in predicting separated and recirculating flows but may produce non-physical viscosities in mixed rotating and stationary flows. It is generally more robust and efficient across a range of applications. In contrast, the SST k-ω model is well-suited for low Re flows with significant separation. It benefits from a combination of models to transition from the k-ω model near the wall to the k-ε model in the outside boundary layer, combining the strengths of both models for improved accuracy across a wider range of flow regimes (Hasan *et al.,* 2025; Karkoulias *et al.,* 2022; Siddiqi and Lee, 2019). It excels in accuracy for flows that experience separation. The measured lift and drag coefficients are presented in Equations 6 and 7, respectively (Mousa *et al.,* 2022).

$$C_D = \frac{2F_D}{\rho V A} \quad (6)$$

$$C_L = \frac{2F_L}{\rho V A} \quad (7)$$

where C_D and C_L are the coefficients of drag and lift forces, respectively, F_D and F_L are the drag and lift forces, respectively, and A is the reference area. The reference area for a 3D wing is the planform area.

A. Wing CAD Model

Due to symmetry of the wing geometry, only half of it was used for the CFD analysis. While Figure 1 present the overall CAD model of the IU-18 UAV, Figure 2 present the IU-18 wing. Detailed specifications are listed in Table 1.

Table 1: Features of the wing of the IU-18 UAV.

Parameter	Value
Area	10.36 m²
Leading-edge sweepback angle	4.39°
Aspect ratio	11.68
Taper ratio	0.42
Span	11 m
Trailing edge sweep angle	4.45°
Fitness ratio	13.0
Root chord length	1.20 m
MAC	0.90 m
Anhedral	3°
Tip chord length	0.50 m
Twist	-2°

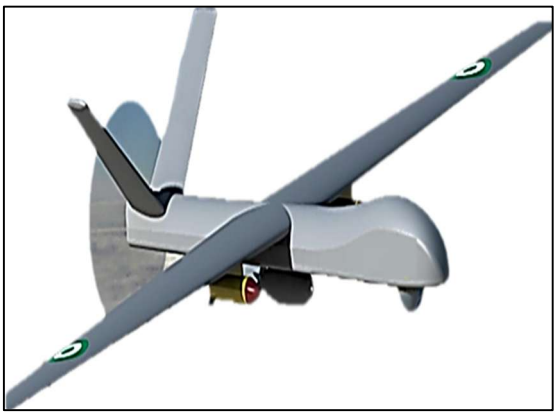

Figure 1. IU-18 UAV overall CAD model

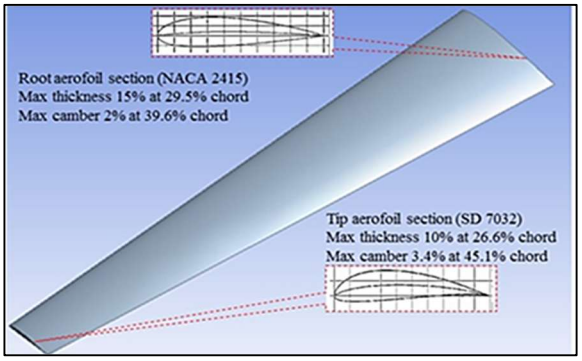

Figure 2. IU-18 UAV wing model

B. Numerical Setup

1) Geometry design modeller

Figure 2 illustrates the virtual computational domain (CD) for the simulation surrounding the geometric model under investigation, in which the basic flow equations are discretized and solved using the numerical method. It is one of the factors affecting the CFD result (Utomo *et al.,* 2024). A C-type CD was chosen for its simplicity and time-saving advantages (Pranto and Inam, 2020). It is dimensionally produced with extended length to the wing chord length, C, to minimize the boundary effect (Mahmud and Mohamad, 2013; Pranto and Inam, 2020). This selection was based on the study's specific requirements for efficiently analyzing fluid dynamics within the given CD.

2) Boundary conditions

The CD employs an 'Inlet Velocity' condition on the front face to represent the free-stream flow, and a 'Pressure Outlet' on the rear face for outflow. Figure 3 shows the applied boundary conditions. The top and bottom rectangular faces are defined as 'Walls' with a no-slip condition, while the wing surface is assigned a 'slip wall' condition. For each AoA, flow velocity vectors were computed to simulate changes in flight AoA.

3) Meshing

For the wing model, an unstructured mesh was created, and modifications were implemented to enhance grid quality. A grid independence check was performed to verify that the mesh size did not affect the accuracy of the solution. Figure 3 displays the final mesh, comprising 86,546 nodes and 482,214 fluid elements, which was used for the subsequent CFD analysis. Simulations utilizing finer grids indicated only a slight effect on the drag and lift coefficients, with variations falling within an acceptable range (refer to Table 2).

Table 2: Grid independence test results.

Grid size	AoA	Nodes	Elements	C_D	C_L
Coarse	0°	67,654	376,935	0.044	0.321
Finer	0°	86,546	482,214	0.026	0.246

4) Setup

Table 3 lists the boundary conditions for the simulation, consisting of the UAV cruising conditions and the surrounding air properties.

Table 3: Input boundary conditions

Parameter	**Value**
Speed (m/s)	46
Re	1.92E6
Pressure (kPa)	57.182
Viscosity ($kg/m*s$)	1.66E-5
Density (kg/m^3)	0.771
Temperature (K)	258.43

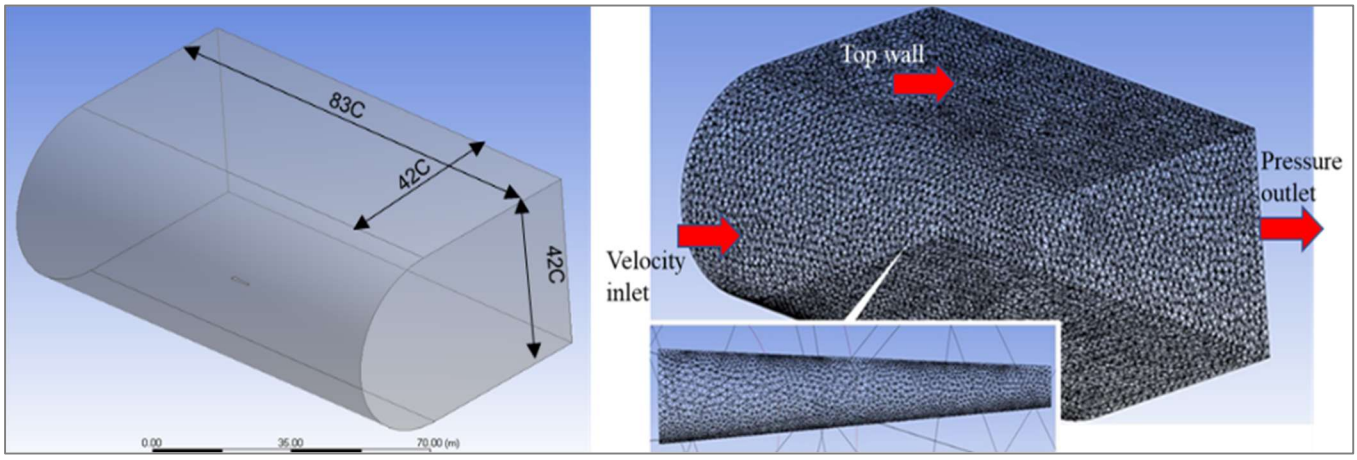

Figure 3. Computational domain (left) and the unstructured grid divisions (right)

C. Initialization of the Solution

The solution process began with "Hybrid Initialization", which combines boundary interpolation and Laplace equation solving to generate an initial velocity field suitable for complex geometries and a smooth pressure distribution within the CD. Other variables, including velocity, pressure, turbulence, and volume of fluid (VOF), were initialized using domain averages or predefined values (ANSYS Inc, 2013). Seven simulations were run for each of the turbulence models, corresponding to AoA from 0° to 24° at an interval of 4° increments. Lift and drag coefficients were recorded at every iteration, and convergence was closely monitored. To enhance convergence, the Root-Mean-Square (RMS) residual threshold was set to 10^{-6}. Where convergence was not achieved within the set criteria, the simulations proceeded until residuals exhibited minimal fluctuations, indicating a stabilized solution.

III. RESULTS AND DISCUSSION

This section presents the simulation results and a detailed analysis of the wing aerodynamic performance of the IU-18 UAV. Key parameters analyzed include lift and drag coefficients, drag polar, surface pressure distribution, and velocity vectors, which are critical indicators of aerodynamic behavior. The study examined AoA from 0° to 24° in 4° increments. However, for clarity, air pressure contours and velocity vectors on the surface of the wing are presented at 8° intervals using the freestream velocity of 46 m/s. The simulation assumes a stationary wing exposed to incoming airflow, equivalent to the wing moving through still air. Each case was iterated until convergence was achieved.

A. Flow Characterization

Figure 4(a-d) illustrates the surface pressure distributions for the realizable $k-\varepsilon$ and SST $k-\omega$ turbulence models. These visualizations provide insight into flow behavior, highlighting regions of high and low pressure, as well as areas of stagnation and accelerated flow around the wing as the AoA changes. From the pressure plots, Figure 4, low-pressure regions (blue and green shades) near the trailing edge diminish as AoA increases, giving way to high-pressure zones (red shades). The pressure distribution varies with change in AoA for each turbulence model. As expected, pressure peaks at the leading edge across all cases and increases with AoA. This rise in pressure explains the increased drag at higher AoA, while lifts tend to decrease beyond a certain point. The maximum static pressure observed is 808 Pa for the realizable $k-\varepsilon$ turbulence model and 797 Pa for the SST $k-\omega$ turbulence model. Toward the trailing edge, pressure builds up significantly. The minimum pressure recorded is 723 Pa for the realizable $k-\varepsilon$ turbulence model and 720 Pa for the SST $k-\omega$ turbulence model.

Figure 5 shows that increasing the AoA from 0° to 24° results in a decrease in airflow velocity over the wing surface across all the turbulence models used. Bernoulli's principle is evident in the flow behavior around the IU-18 UAV wing, confirming the theoretical basis for external aerodynamics. For all the

AoA, the maximum airflow velocity observed was 101 m/s for the realizable $k-\varepsilon$ turbulence model and 100 m/s for the SST $k-\omega$ turbulence model. The minimum velocities were 64.8 m/s and 65.4 m/s, respectively. These results are consistent with previous studies (Cao, 2011; Kandil and Elnady, 2017; Manikantissar and Ankur, 2017; Meyers, 2018; Triet *et al.,* 2015), which have reported similar trends of increasing velocity and decreasing static pressure as AoA decreases, and vice versa, supporting Bernoulli's theorem.

B. Aerodynamic Coefficients

Figure 6 illustrates the drag coefficient results obtained from the simulation by applying the turbulence models. The results presented the drag coefficient values obtained from 0° to 24° in 4° increments. Figure 6 shows that the drag coefficient increases progressively, directly proportional to AoA, for all turbulence models in a similar trend. However, at the extreme AoA, the SST $k-\omega$ turbulence model predicted a higher value. Siddiqi and Lee (2019) have reported a similar behavior of the selected turbulence models. The drag increase is expected, as higher AoA increases the wing's exposed surface area to the freestream, leading to greater pressure. Additionally, lift-induced drag increases with AoA due to the demand for higher lift.

AoA	k − ε model	SST k − ω model
0°	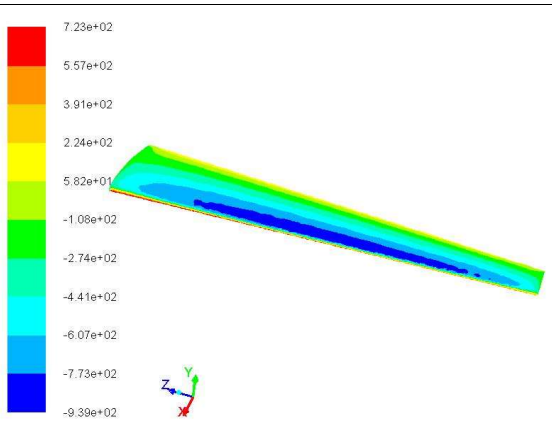	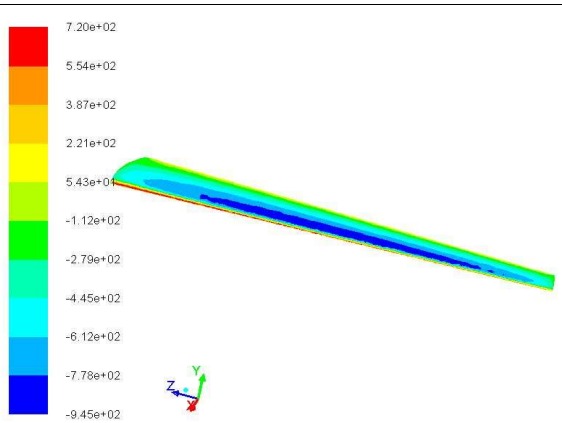
8°	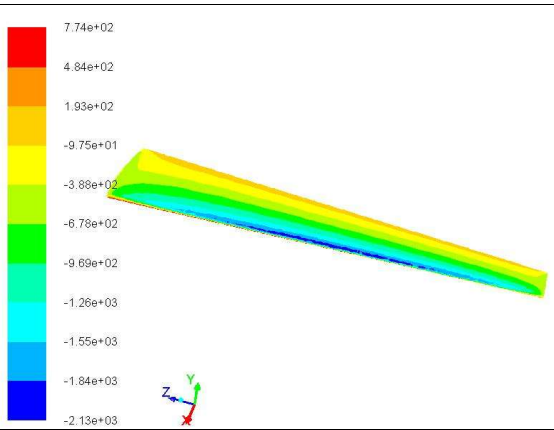	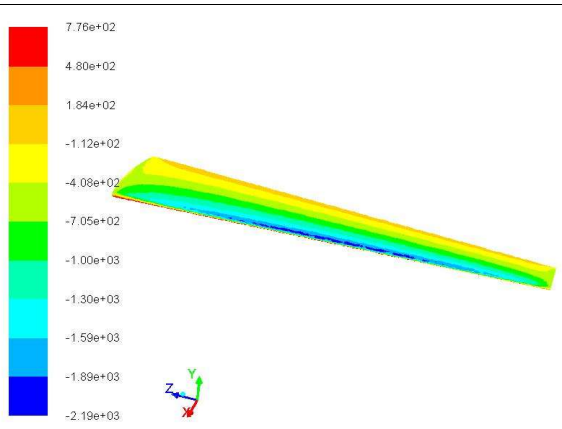
16°	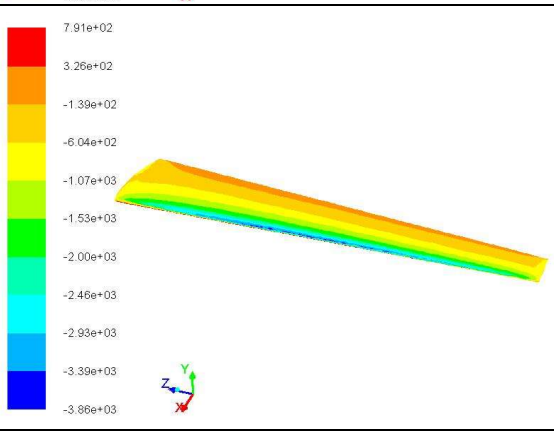	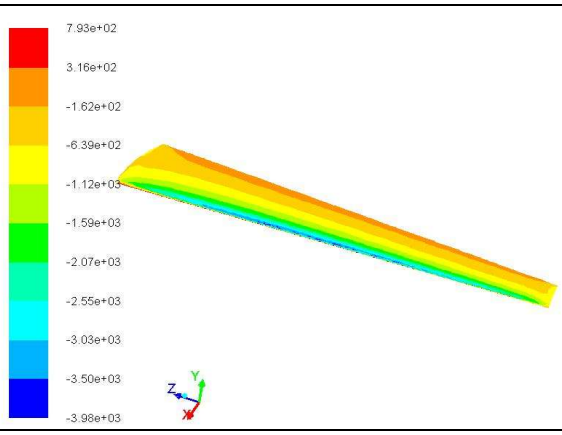

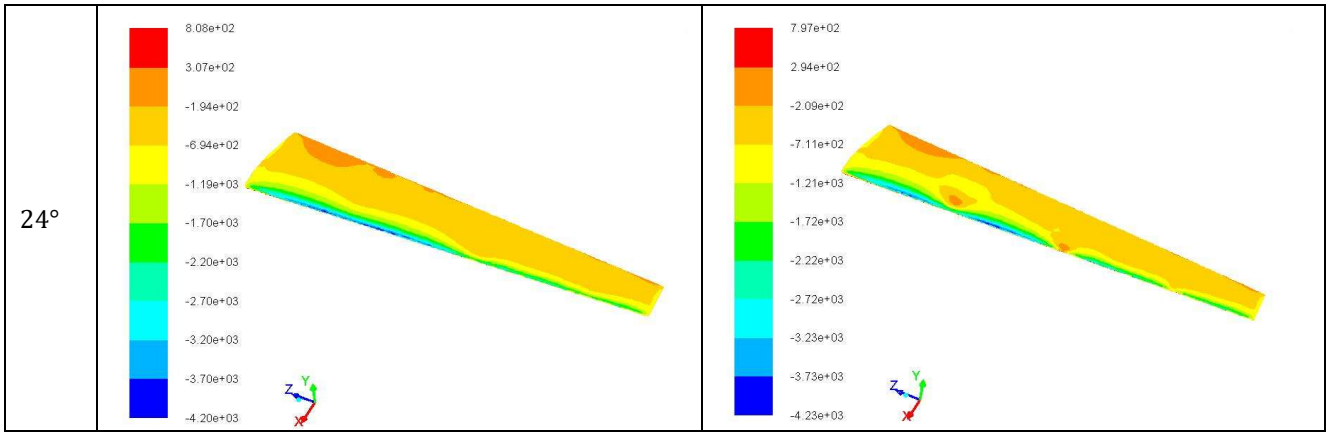

Figure 4. Air static pressure contours on the surface of the IU-18 UAV wing

AoA	k – ε model	SST k – ω model
0°	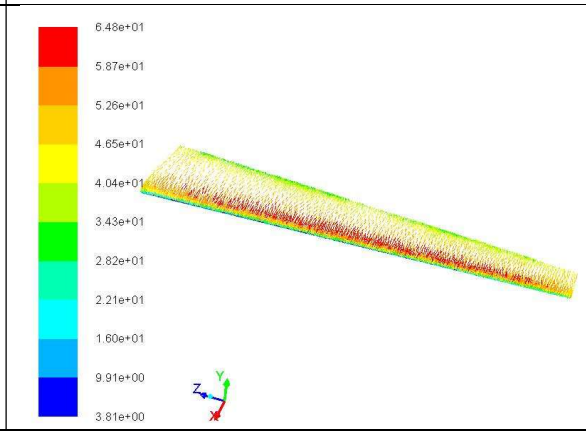	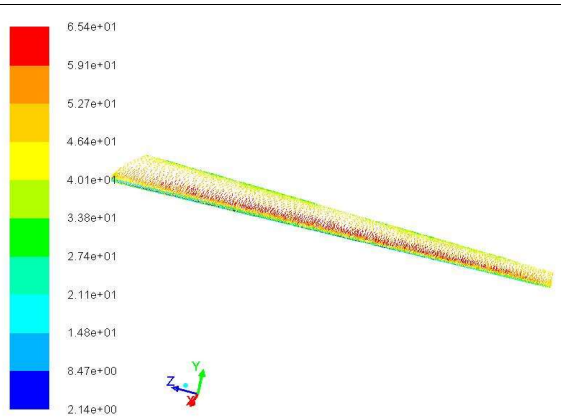
8°	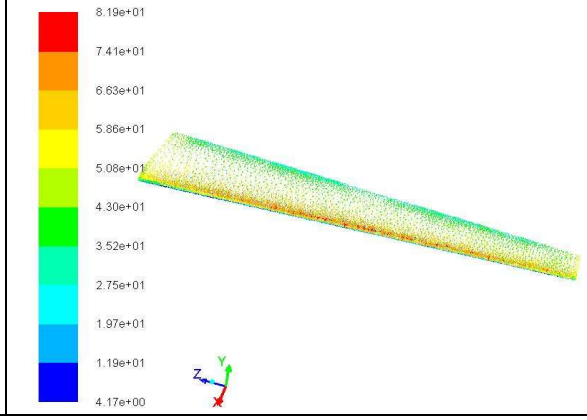	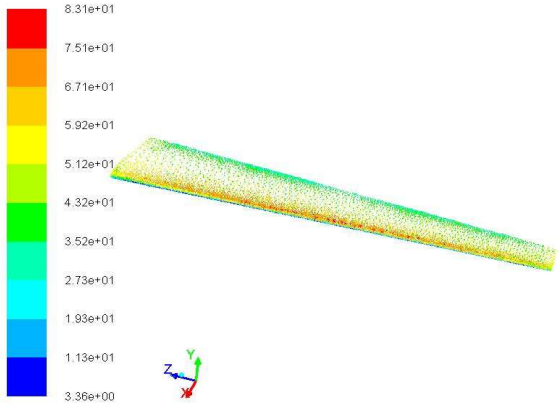

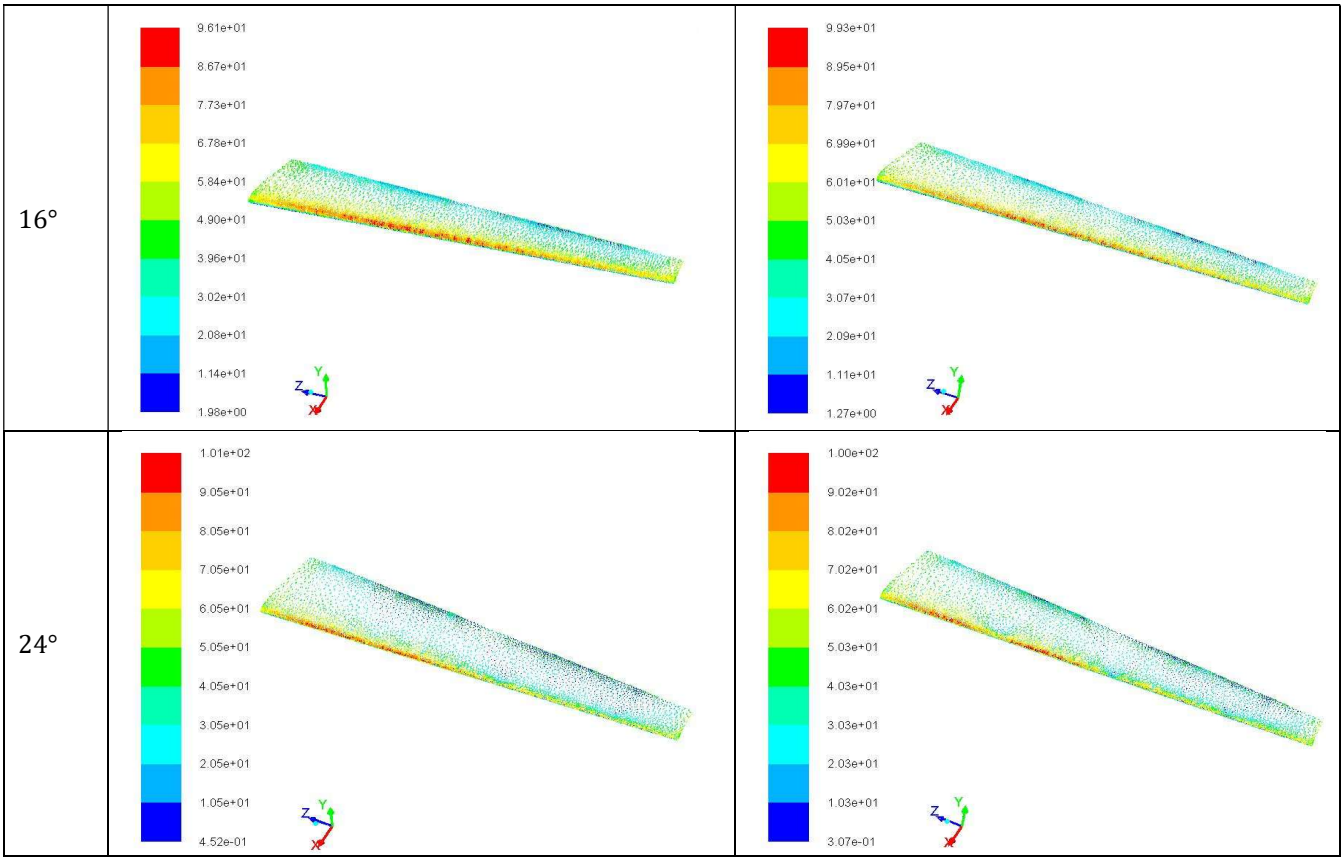

Figure 5. Air velocity vectors on the surface of the IU-18 UAV wing

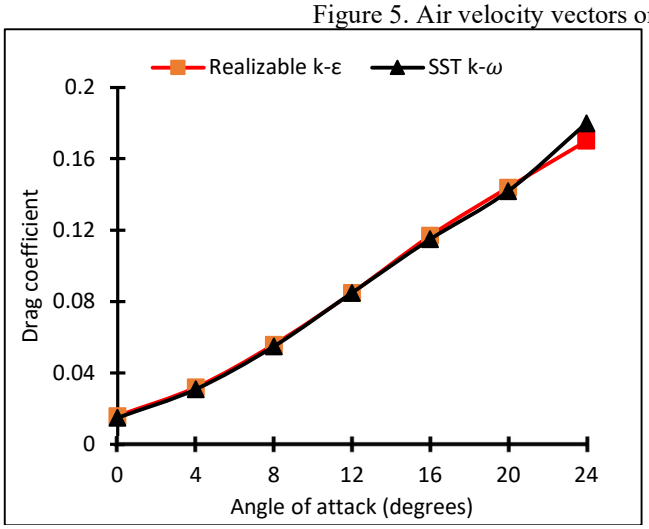

Figure 6. Drag coefficients versus AoA

The minimum drag coefficients, 0.016 and 0.015, occur at 0°AoA for the realizable $k-\varepsilon$ and SST $k-\omega$turbulence models, respectively, while the maximum values of 0170 and 0.180 are observed at 24° AoA. Hamza (2020), using the Athena Vortex Lattice (AVL) method, reported a drag coefficient of 0.030 at 0° AoA for the IU-18 UAV wing. This value is reasonable, as the study considered both the wing and the tail sections, with the tail inherently contributing to higher drag.

Figure 7 illustrates the change of lift coefficient with AoA. At 0° AoA. Both these models predicted almost equal values. The SST k-ω and the realizable k-ε turbulence models predict a minimum lift coefficient of 0.265 and 0.264, respectively. In comparison, Hamza (2020), using the AVL method for both the wing and tail sections of the IU-18 UAV, reported a lift coefficient of 0.377 at 0° AoA. Likewise, the analytical method used by (Jemitola and Abbe, 2018) estimated the lift coefficient at 0.389. While the lift increases initially, it peaks at 16°AoA and decreases beyond that point for all the models. This indicates that 16° is the critical AoA, where the wing produces maximum lift. Beyond this angle, a stall occurs as airflow begins to separate from the wing surface. The observed flow separation is due to low inertia and high viscosity, triggered by a strong adverse pressure gradient that increases with AoA. As the flow separates from the wing surface, the lift decreases. At the critical AoA (16°), the realizable $k-\varepsilon$ and SST $k-\omega$ turbulence models yielded maximum lift coefficients of 0.581 and 0.587, respectively. Flow separation under stall conditions results in a reduced pressure difference between the upper and lower wing surfaces, decreasing lift and increasing drag. While some lifts are still generated at higher AoAs, most of the aerodynamic force is redirected as lift-induced drag. Therefore, flight beyond the critical AoA is unsafe. An analytical design of the IU-18 UAV yielded a critical lift coefficient of 0.74 at 15.6° AoA (Jemitola and Abbe, 2018). It is essential to highlight that this increased value

of critical AoA, derived analytically, applies to the entire UAV.

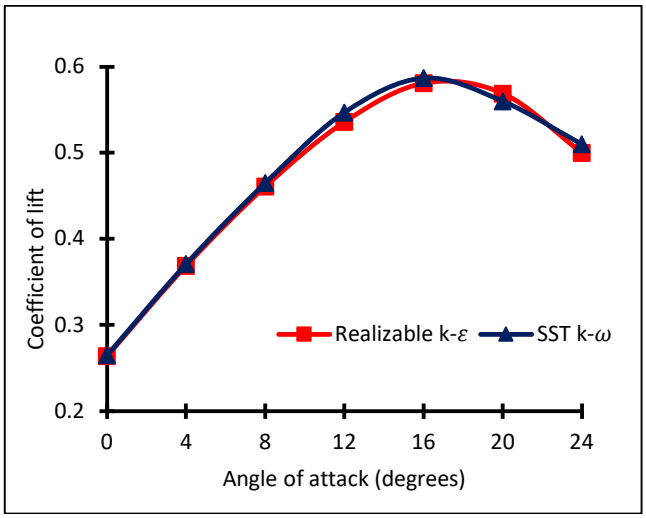

Figure 7. Lift coefficients versus AoA

The lift-to-drag coefficient ratio, also known as aerodynamic efficiency, was determined and presented. Figure 8 depicts the effect of aerodynamic efficiency with AoA. All the models exhibit a similar trend. The highest aerodynamic efficiency occurs at 0°AoA,16.5 and 17.67 for the realizable $k-\varepsilon$ and SST $k-\omega$ turbulence models, respectively. Beyond this angle, efficiency drops sharply as drag increases more rapidly than lift. Although lift increases beyond0°, the reduced efficiency implies higher fuel consumption and environmental impact, making it economically unfavorable for cruising. The lowest aerodynamic efficiencies, 2.94 and 2.83, are observed at 24° AoA for the realizable $k-\varepsilon$ and SST $k-\omega$ turbulence models, respectively.

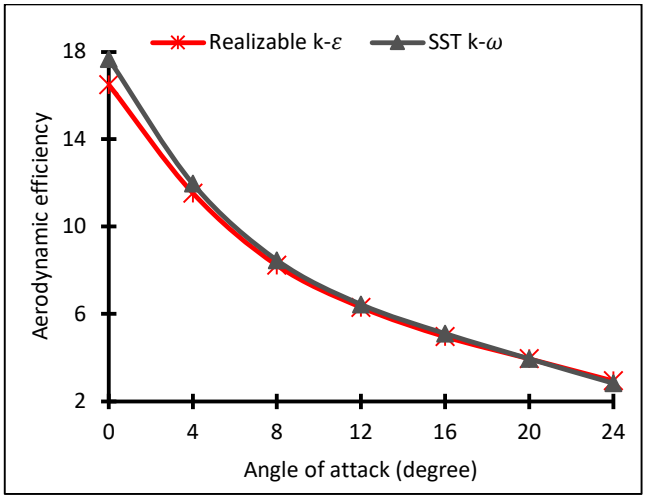

Figure 8. Aerodynamic efficiency versus AoA

C. Results Summary and Validation

Table 4 compare the summarize CFD results with the analytical and Athena vortex lattice (AVL) methods by (Jemitola and Abbe, 2018) and (Hamza, 2020), respectively results at 0° AoA.

Table 4. Results summary

Method	C_D	C_L	C_L/C_D
Analytical	0.052	0.780	15.0
AVL	0.021	0.755	35.95
$k-\varepsilon$ realizable	0.032	0.528	16.50
$SST\ k-\omega$	0.030	0.530	17.67

In all the methods, the analytical method presented the highest C_D and C_L of 0.52 and 0.780, respectively. As the table shows, the AVL method result presented the greatest aerodynamic efficiency of 35.95%, while the analytical method presented the least aerodynamic efficiency of 15.0% at 0° AoA. For the analytical and AVL methods, the tail configuration surfaces were put into consideration in estimating the C_D and C_L respectively. Therefore, the inconsistency of the CFD results with the analytical and AVL methods could be attributed to the fact that the CFD method overlooked the tail configuration surfaces, which will significantly affect the overall CFD results obtained.

IV. CONCLUSION

This study applied the CFD to evaluate the aerodynamic performance of the IU-18 UAV wing across various AoA, focusing on its cruising flight phase. The analysis revealed that AoA significantly influences lift, drag, and overall aerodynamic efficiency. As AoA increases, the lift coefficient rises until it peaks at 16o, after which it declines, indicating the stall point. Simultaneously, drag increases with AoA, reducing aerodynamic efficiency and fuel consumption. The highest efficiency occurs at 0o AoA, while the lowest is observed at 24o, consistent across turbulence models tested. These results confirm that 16o AoA marks the stall angle, aligning with design expectations. The study compares the performance of the models. While the models differ in complexity, they produced similar trends in predicting aerodynamic behavior. The comparison with available analytical design data shows good agreement, validating the CFD approach used. This research enhances the understanding of the IU-18 UAV wing's aerodynamic behavior and demonstrates the effectiveness of CFD in predicting flow characteristics at different AoA. It offers valuable insights into airflow phenomena and contributes to the broader effort of optimizing UAV performance.

AUTHOR CONTRIBUTIONS

A Isah: Carried out the analysis and writing of the manuscript. **MS Lawal:** Supervision, interpretation of the results, writing and review of the of the manuscript**. I Yahuza:** Supervision and review of the manuscript. **A Na'inna:** Review

of the manuscript. All authors read and approved of the final manuscript.

ACKNOWLEDGEMENT(S)

The authors thank the Air Force Research and Development Center (AFRDC) and the Air Force Institute of Technology (AFIT) for offering numerous design input parameters throughout the study.

REFERENCES

Aftab, S.M.A., Rafie, A.S.M., Abdul Razak, N.A., Ahmad, K.A., (2016). Turbulence Model Selection for Low Reynolds Number Flows. PLoS ONE 11, 1–15.

Ali, I., Hussain, T., Unar, I.N., Kumar, L., Ahad, I.U., (2024). Turbulence model study for aerodynamic analysis of the leading edge tubercle wing for low Reynolds number flows. Heliyon 10.

Ananda, G.K., Sukumar, P.P., Selig, M.S., (2015). Measured aerodynamic characteristics of wings at low Reynolds numbers. Aerospace Science and Technology 42, 392–406.

Anderson, J.D., (2011). Fundamentals of Aerodynamics, Sixth. ed. McGraw-Hill Education, New York.

ANSYS Inc, (2013). ANSYS Fluent Theory Guide.

Arunkumar, K., Chinthamani, P., Nema, D., Nandhini, R., P, N.S., (2018). Performance Analysis of Winglet Using CFD. In: International Conference on Aeronautics, Astronautics and Aviation (ICAAA). pp. 151–157.

Bardera, R., Rodríguez-Sevillano, Á.A., Barroso-Barderas, E., Matías-García, J.C., (2024). CFD study of the effect of leading-edge tubercles on the aerodynamic characteristics of a small UAV based on eppler 186 airfoils. Results in Engineering 23.

Cakir, M., (2012). CFD Study on Aerodynamic Effects of a Rear Wing/Spoiler on a Passenger Vehicle. Santa Clara University, California.

Cao, H., (2011). Aerodynamics Analysis of Small Horizontal Axis Wind Turbine Blades by Using 2D and 3D CFD Modelling. University of the Central Lancashire.

Eftekhari, S., Al-obaidi, A.S.M., Mahdi Al-Obaidi, A.S., (2019). Investigation of a NACA0012 Finite Wing Aerodynamics at Low Reynold's Numbers and 0° to 90° Angle of Attack. J Aerosp Technol Manag 11: e1519, 1–11.

Hamza, A., (2020). Flight Performance of ICHOKU-18 Unmanned Aerial Vehicle. Air Force Insitute of Technology, Kaduna.

Hasan, M., Redonnet, S., Zhongmin, D., (2025). Aerodynamic optimization of aircraft wings using machine learning. Advances in Engineering Software 200, 103801.

İnan, A.T., Ceylan, M., (2024). Aerodynamic Analysis of Fixed-Wing Unmanned Aerial Vehicles Moving in Swarm. Applied Sciences 14.

Iqbal, Z., Al-faruk, A., Islam, A., (2025). Experimental Analysis of Aerodynamic Characteristics of NACA 0012 Wing Model with Multiple Winglets. Journal of Engineering Advancements 06, 22–30.

Isah, A., Abdulazeez, M.U., Aliyu, M., Yahuza, I., (2022). Study of Aerodynamic Performance of Rear Trunk Lip Spoiler on a Passenger Car. FUW Trends in Science & Technology Journal 7, 1017–1022.

Isah, A., Abdulazeez, M.U., Aliyu, M., Yahuza, I., (2025). Investigating the Effect of a Passenger Vehicle Front Profile on Aerodynamic Performance. Journal of Sustainable Engineering and Technology 1, 215–224.

Ismail, N.A., Usman, K.M., Balogun, M.B., Abdullahi, M., Faru, F.T., Ibrahim, I.U., (2020). Effect of Angle of Attack on Lift, Drag, Pitching Moment and Pressure Distribution of NACA 4415 Wing Effect. Journal Of Science Technology and Education 8, 31–44.

Isah, A., Rahim, A., Talib, A., Faisal, M., Hamid, A., Gires, E., Mat, S., (2025). Conceptual Design of Hydrogen Fuel Cell-Powered Aircraft: A Review. Journal of Aeronautics, Astronautics and Aviation 57, 531–556.

Jemitola, P.O., Abbe, G.E., (2018). Medium Altitude Long Endurance Surveillance Aircraft IU-18 Project Specification.

John, J.B., Russell, M.C., (2014). Aerodynamics for Engineers, Sixth Edit. ed. Pearson Education Limited, United Kingdom.

Kandil, M.A.F., Elnady, A.O., (2017). Performance of GOE-387 Airfoil Using CFD. International Journal of Aerospace Sciences 5, 1–7.

Karkoulias, D.G., Tzoganis, E.D., Panagiotopoulos, A.G., Acheimastos, S.-G.D., Margaris, D.P., (2022). Computational Fluid Dynamics Study of Wing in Air Flow and Air–Solid Flow Using Three Different Meshing Techniques and Comparison with Experimental Results in Wind Tunnel. Computation 10, 34.

Khuntia, S.K., Ahuja, A.S., Base, N., (2018). Optimal Design and CFD Analysis of Wing of a Small-Scale UAV to Obtain Maximum Efficiency. International Journal of Computer Application 1, 148–164.

Kulshreshtha, A., Gupta, S.K., Singhal, P., (2020). FEM/CFD analysis of wings at different angle of attack. Materials Today: Proceedings 26, 1638–1643.

Lawal, M.S., Thomas, S., Udeagulu, C., Jemitola, P.O., (2015). Prediction of Aerodynamic Paramaters and Pressure Distribition of the Wing of Gulma UAV. In: 3rd International Symposium on Engineering and Natural Science (ISEAN). Beijing.

Lei, Y., An, X., Pan, Y., Zhou, Y., Chen, Q., (2024). Prediction of pressure distribution and aerodynamic

coefficients for a variable-sweep wing. Aerospace Science and Technology 155, 109706.

Mahmud, S., Mohamad, W., (2013). Introduction to ANSYS Workbench.

Manikantissar, Ankur, G., (2017). CFD Analysis of Conceptual Aircraft Body. International Research Journal of Engineering and Technology (IRJET) 4, 217–222.

Merryisha, S., Rajendran, P., (2019). Experimental and CFD Analysis of Surface Modifiers on Aircraft Wing: A Review. CFD Letters 11, 46–56.

Meyers, L.M., (2018). Analysis of Lift and Drag Forces on the Wing of the Underwater Glider. Cape Peninsula University of Technology.

Mishra, P., Aharwal, K.R., (2018). A review on selection of turbulence model for CFD analysis of air flow within a cold storage. IOP Conference Series: Materials Science and Engineering 402.

Mousa, N.A., Attia, O.H., Mahmood, H.A., Adam, N.M., (2022). Optimization Efficiency of the Aircraft Wing of Cessna 172 Skyhawk by Absorbent Adverse Pressure Using Tangential Suction Slot Without Vacuum Device. Mathematical Modelling of Engineering Problems 9, 731–738.

Narendiranath, B.T., Parmenshwar, P., Beladiya, A., Bhabhra, A., (2017). CFD Analysis and Comparison using Ansys and Star-CCM+ Of Model Aerofoil Selig 1223. International Journal of Mechanical Engineering and Technology (IJMET) 8, 312–318.

Nigam, P.K., Tenguria, N., Pradhan, M.K., (2017). Analysis of horizontal axis wind turbine blade using CFD. International Journal of Engineering, Science and Technology 9, 46–60.

Pranto, M.R.I., Inam, M.I., (2020). Numerical Analysis of the Aerodynamic Characteristics of NACA-4312 Airfoil. Journal of Engineering Advancements 01, 29–36.

Roy, A., Mallik, A.K., Sarma, T.P., (2018). A Study of Model Separation Flow Behavior at High Angles of Attack Aerodynamics. Journal of Applied Computational Mechanics 4, 318–330.

Siddiqi, Z., Lee, J.W., (2019). A computational fluid dynamics investigation of subsonic wing designs for unmanned aerial vehicle application. Proceedings of the Institution of Mechanical Engineers, Part G: Journal of Aerospace Engineering 233, 5543–5552.

Triet, N.M., Viet, N.N., Thang, P.M., (2015). Aerodynamic Analysis of Aircraft Wing. VNU Journal of Science: Mathematics – Physics 31, 68–75.

Utomo, M.S. T.S., Yohana, E., Mahendra, C., Utama, I.Y., (2024). Analysis of blended winglet parameters on the aerodynamic characteristics of NXXX aircraft using Computational Fluid Dynamics (CFD). Results in Engineering 24, 102901.

Yuichi, K., Ryo, I., Midori, M., Keisuke, S., (2020). Numerical Study of Flowfield Around a Multislotted High-Lift Wing. Journal of Aircraft 1–7.

Zharif, M., Taib, I., Imran, M.N., Alif, N.A., Kamilia, N., (2024). Analysis of Airflow Characteristics of Different Models of Unmanned Aerial Vehicles. Semarak Journal of Thermal-Fluid Engineering 1, 9–15.